

www.acsanm.org Article

Interactions of Ti₃C₂ MXene with Aqueous Zwitterionic Biological Buffers: Implications for Applications in Biological Systems

Swapnil B. Ambade, Laura A. Kesner, Mohammed K. Abdel-Rahman, D. Howard Fairbrother, and Zeev Rosenzweig*



Cite This: https://doi.org/10.1021/acsanm.3c00666



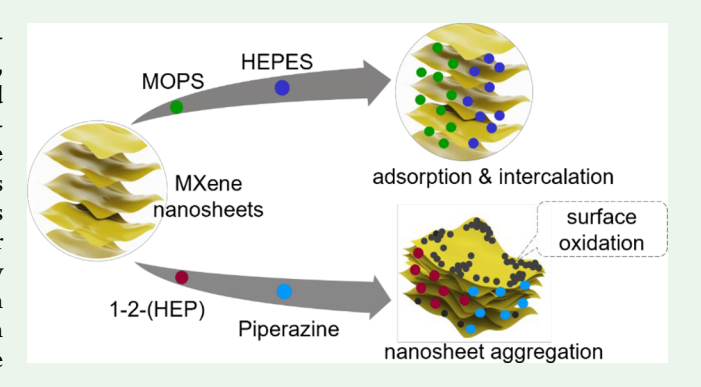
ACCESS I

III Metrics & More

Article Recommendations

SI Supporting Information

ABSTRACT: MXenes, a family of ultrathin layered two-dimensional (2D) transition-metal carbides, nitrides, and carbonitrides, are steadily advancing as novel inorganic nanosystems for a broad range of applications. While high conductivity, solution processability, hydrophilic nature, and the presence of various surface functional groups enable the use of 2D MXenes in aqueous systems, applications that involve the use of MXenes in aqueous systems and biological solutions, including but not limited to water treatment, water desalination, and biological assays, are only beginning to emerge. For the successful application of MXene in aqueous systems, their interactions with common aqueous solution constituents must be better understood. This paper describes the structural and functional properties of $Ti_3C_2T_x$ ($Tx = O^-$, OH^- ,



 F^-) MXenes in N-substituted commonly used biological buffers like N-(2-hydroxyethyl)-piperazine-N'-ethanesulfonic acid (HEPES) and 3-(N-morpholino)-propane sulfonic acid (MOPS) and with a series of piperazine-based molecules dissolved in phosphate buffer solutions. Dissolving MXenes in these buffers significantly impacts their optical, structural, and electrical properties. The interactions of $Ti_3C_2T_x$ MXenes with N-substituted zwitterionic buffer molecules are structure-dependent and mostly but not fully reversible. X-ray photoelectron spectroscopy measurements reveal small but measurable surface oxidation through the formation of Ti-O bonds. Our results suggest a complex interaction pattern where some interactions are driven by hydrogen bonding and electrostatic forces, while others involve chemisorption, which results in a permanent impact on the MXene nanosheets. This study is an important step toward understanding the stability of MXenes in complex aqueous media and the impact of interactions of MXenes with nitrogen-containing molecules on MXene properties, which are especially important in applications of MXenes in biological systems. The nature of interactions between MXenes and biological buffer molecules, revealed in our study, suggests that surface chemistry modifications of MXenes are required to preserve their chemical stability and enable their applications in complex biological solutions.

KEYWORDS: Ti_3C_2 MXene, N-(2-hydroxyethyl)-piperazine-N'-ethanesulfonic acid, 3-(N-morpholino)-propane sulfonic acid, zwitterionic biological buffers, intercalation, adsorption, aggregation, oxidation

■ INTRODUCTION

Non-toxic and environmentally friendly titanium-based transition-metal carbide two-dimensional (2D) materials, termed MXenes, 1,2 have attracted significant attention in the materials research community as they add a large number of building blocks to the family of hydrophilic, 3 layered 2D materials. MXenes are a large group of 2D transition-metal carbides, nitrides, and carbonitrides, with the formula $M_{n+1}X_nT_n$ where M represents a transition metal (Ti, V, Nb, Ta, Mo, Zr, Cr, Sc, etc.), X is carbon and/or nitrogen, and n = 1, 2, or 3^{5-15} MXenes are obtained through a top-down synthesis approach of selectively etching a parent non-van der Waals ceramic precursor called MAX phase, where A represents an element from group IIIA to VIA of the periodic table such as Al or Si. Due to the presence of more chemically active metallic M-A

bonds and covalent M–X bonds, highly reactive fluorine-containing etchants must be used to extract monoatomic A-metal layers from the MAX phase forming loosely stacked MX layers. 8,16 These multilayered structures are further expanded normally to the in-plane direction or sheared parallelly to yield atomically thin nanosheets that are unique from the bulk multilayered structures. Such delaminated monolayers of MXenes are characterized by a high density of mobile

Received: February 12, 2023 Accepted: February 24, 2023



electronic carriers, which results in extraordinary metal-like electrical conductivity. By 10,17 Due to their structural and electrical properties, MXenes have already been applied as components of devices in energy storage, sensors, and electronics, wearable electronics, and electromagnetic interference shielding. They have also been used as catalysts and in photothermal therapy and water treatment to remove contaminants.

The aqueous phase synthesis of MXenes adds surface functionalities (represented as Tx in the MXenes' general formula) such as oxygen (O), hydroxyl (OH), fluorine (F), and chlorine (Cl). The capability of MXenes to retain surface charge results in high colloidal stability in aqueous solutions over a broad pH range between 4 and 12.5,8,17,38 These surface functional groups provide anchoring sites for attaching various surface functionalization agents but may also present chemical vulnerabilities. Although, ideally, 2D nanosheets would comprise single monolayers, they often form incompletely exfoliated flakes with a thickness of a small number (<10) of stacked monolayers. When MXenes absorb guest molecules into their interlayer spaces, creating inclusion complexes through intercalation, the surface terminations aid in holding these intercalants intact, weakening the interlayer adhesion and increasing the layer spacing. This process reorganizes the nanosheets into highly controlled nanostructures either by increasing gaps between the densely packed nanosheets or by forming a specifically ordered arrangement of MXene nanosheets over a wide area. 8,17,39 With a negative surface charge, MXenes show high stability in aqueous solution. 40 However, their applications in aqueous media have been limited to date. To increase the use of MXenes in aqueous media, it is essential to understand the interactions between MXene nanosheets and aqueous solution components, especially in complex biological buffer solutions. It should be noted that the presence of dissolved oxygen and water molecules in an aqueous solution could lead to the oxidation of MXene nanosheets, especially of Ti atoms at the defect and edge sites of MXenes.⁴¹ However, this is a more prevalent problem in MXenes synthesized using earlier synthesis methods, resulting in a higher defect density. Recent molecular dynamics simulations of MXenes also show that the attack of water molecules on the basal plane of O-terminated MXenes could lead to hydrolysis of MXenes, which pulls out Ti atoms to the surface, making them more susceptible to oxidation. 42 This study also indicates that converting the surface O into -OH groups and negatively charging the surface prevent hydrolysis and stabilize the surface.

With growing interest in using MXenes in biological and environmental applications, $^{43-45}$ it is important to note that the use of MXenes in biological applications must involve their suspension in more complex aqueous solutions than just water. Therefore, it is critical to understand the interactions of MXene nanosheets with biological buffers commonly used in biological applications. This paper focuses on the behavior of $\text{Ti}_3\text{C}_2\text{T}_x$ MXenes in two widely used nitrogen (N)-substituted zwitterionic biological buffers: 2-[4-(2-hydroxyethyl) piperazin-1-yl] ethane-1-sulfonic acid (HEPES), which contains a piperazine ring terminated with sulfonyl and hydroxyl groups, and (3-(N-morpholino) propane sulfonic acid (MOPS), which contains a morpholine ring terminated with a sulfonyl group. To elucidate the role of the sulfonyl and hydroxyl groups in HEPES buffer, MXenes were also solubilized in the HEPES—analogue solutions of piperazine and 1-2-(hydroxyethyl)

piperazine (1-2-HEP). Nitrogen containing buffer and biological molecules are ubiquitous in biological systems, and their presence could impact MXene chemical stability and performance in a multitude of biological applications, for example, electrochemical and plasmonic biosensors 46-48 and photothermal and drug delivery technologies. 43-45,49,50 Our study shows that MXenes interact with N-substituted biological buffer molecules and that these interactions impact the structural and functional properties of MXenes, most importantly their electrical conductivity. This study is an important step in understanding the behavior of MXenes in biological solutions.

■ EXPERIMENTAL SECTION

Materials and Reagents. The Ti₃AlC₂ MAX phase was procured from the Gogotsi Group, Drexel University, USA. Hydrofluoric acid (HF), hydrochloric acid (HCl), and lithium chloride were purchased from Sigma-Aldrich. HEPES and MOPS buffers, piperazine, and 1-2-(hydroxyethyl) piperazine (1-2-HEP) were purchased from Sigma-Aldrich. All chemicals were used as received without any further purification. The polypropylene membrane, 3501 Coated PP, was purchased from Celgard LLC Co. (Charlotte, NC, USA).

 $Ti_3C_2T_x$ MXene Synthesis. The synthesis of $Ti_3C_2T_x$ MXenes was carried out following recently described synthesis protocols. 40,51-5 Typically, a sample of the Ti₃AlC₂ MAX phase was selectively etched by slowly adding Al-rich Ti₃AlC₂ (1 g, <75 μm particle size) to an etchant solution containing HF (12 M) and HCl (15 M) in a 50 mL plastic bottle over the course of \approx 5 min due to the exothermic nature of the reaction. The suspension was stirred at 300 rpm with a polytetrafluoroethylene-coated stir bar at 35 °C for 24 h in a loosely capped polyethylene terephthalate bottle. The resulting suspension was washed multiple times via centrifugation at 3500 rpm for 5 min with deionized (DI) water in a 50 mL centrifuge tube until the pH reached 7. Following washing, the multilayered MXenes were further delaminated by stirring in 5 wt % lithium chloride solution. The stable suspension comprising monolayered MXenes was obtained by centrifuging the delaminated MXene at a lower speed of 3500 rpm for 5 min each time, until a dark clear supernatant was obtained. The obtained dark supernatant was further subjected to high-speed centrifugation at 10,000 rpm for 2 h to concentrate the solution. The as-obtained concentrated MXene nanosheets were finally dispersed in a 50 mL Millipore water solution to obtain a stable colloidal suspension of concentrations as high as 25 mg mL⁻¹.

Interactions between $Ti_3C_2T_x$ MXene Nanosheets and Zwitterionic Buffers and Their Analogues. The interaction studies between MXene nanosheets and zwitterionic buffers and their analogues were carried out by adding $100~\mu\text{L}$ of $25~\text{mg mL}^{-1}~\text{Ti}_3C_2T_x$ MXene colloid samples to 20~mL glass vials containing 10~mL of DI water, 10~mL solutions of HEPES and MOPS buffers of varying concentrations between 1~and~10~mM, and 10~mL of piperazine and 1-2-HEP solutions of varying concentrations between 0.5~and~2.0~mM. The MXene-containing solutions were kept under magnetic stirring of 500~rpm at room temperature for 24~h. Following exposure to the N-containing buffers and prior to their analysis by X-ray or electron-based spectroscopies the MXene nanosheets were washed three times by centrifugation at 3500~rpm to remove excess buffer and buffer analogue molecules. The final suspension was vacuum-filtered on polypropylene membranes (Celgard, 3501) and the as-obtained free-standing films were dried under vacuum over at 110~°C for 24~h.

Characterization of MXenes. X-ray diffraction (XRD) (Rigaku HyPix-3000 diffractometer) measurements were conducted on freestanding films using a monochromatic Cu $K\beta$ X-ray source. Survey scans were conducted from 4 to 70° with a step size of 0.03° at 1.2°/min. All films (before and after washing) were dried prior to XRD measurements. The thickness of films was measured with a three-dimensional laser scanning microscope (KEYENCE, VX-X1000). UV—vis spectra of MXene solutions were obtained using an Agilent Cary 3500 UV—vis spectrophotometer with a wavelength range of

ACS Applied Nano Materials www.acsanm.org Article

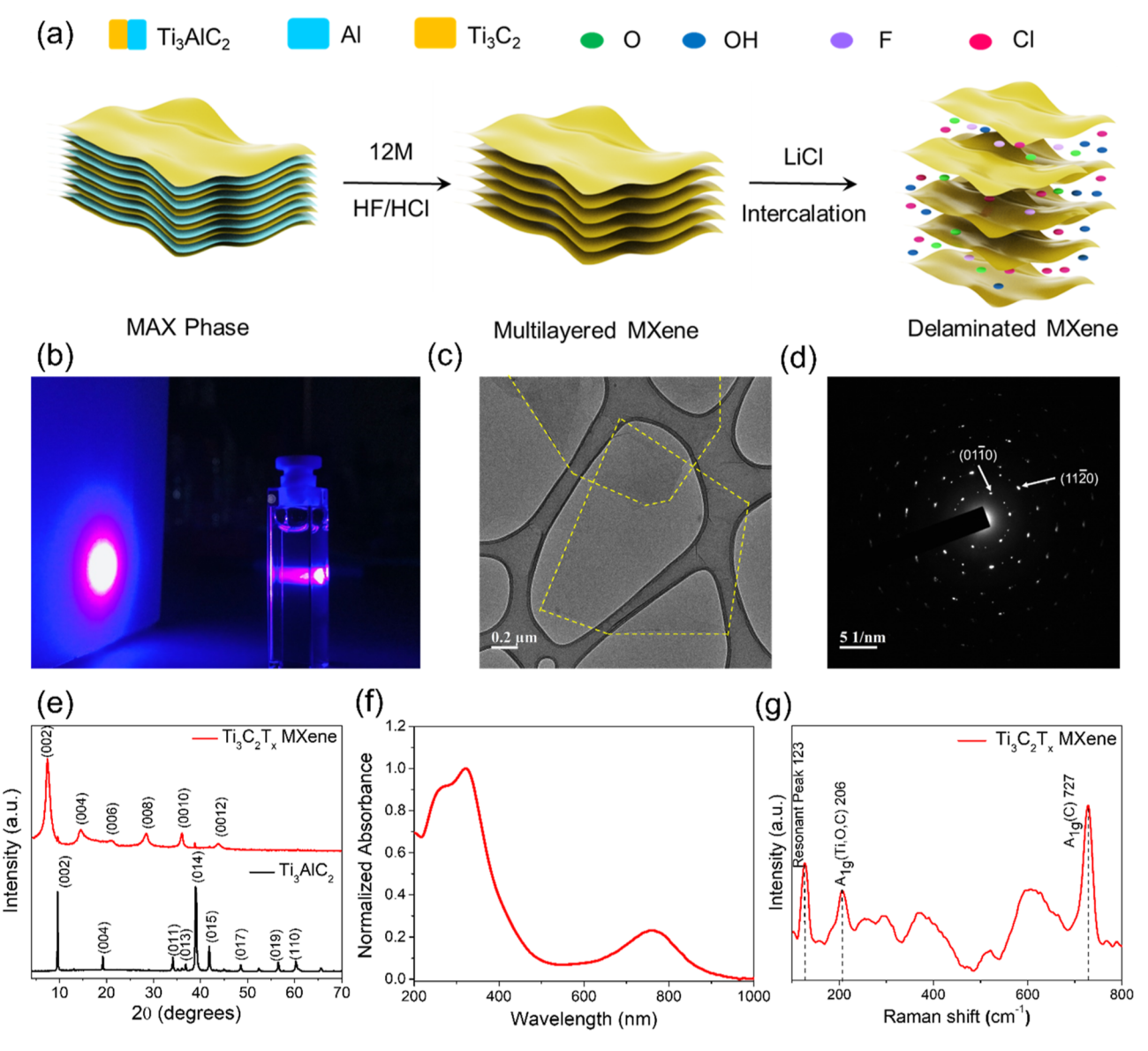


Figure 1. (a) Schematic illustration of the synthetic route of $Ti_3C_2T_x$ MXenes using the mixed acid (HF + HCl) method, (b) Tyndall effect in the as-synthesized MXenes, (c) a representative TEM image (highlighted region) with a scale bar of 0.2 μ m, (d) a SAED pattern, (e) XRD pattern, (f) UV–vis spectrum, and (g) Raman spectrum of $Ti_3C_2T_x$ MXene. These MXene nanosheet characterization measurements are consistent with previous studies and indicate the presence of high-quality MXenes.

200-1000 nm. Structural characterization of MXene nanosheets was carried out using transmission electron microscopy (TEM) (JOEL JEM-ARM200F), selected area electron diffraction (SAED), and fieldemission scanning electron microscopy (Hitachi S4800). TEM samples were prepared by drop-casting solutions of Ti₃C₂T_x MXene nanosheets in DI water (MXene-DI water), HEPES (MXene-HEPES), MOPS (MXene-MOPS), piperazine (MXene-Piperazine), and 1-2-hydroxyethyl piperazine (MXene-1-2-HEP) on lacey carbon TEM copper grids. The grids were then placed in a desiccator to dry the samples completely. X-ray photoelectron spectroscopy (XPS) was conducted on the free-standing MXene films using a VersaProbe 5000 X-ray photoelectron spectrometer with a monochromatic Al K-Alpha (Al K α) 1486.2 eV X-ray source. High-resolution Ti 2p, C 1s, F 1s, O 1s, N 1s, and Fermi energy region spectra were recorded using a pass energy of 23.5 eV and an energy resolution of 0.05 eV. Survey spectra were recorded using a pass energy of 117 eV and an energy resolution of 0.5 eV. Quantification and peak fitting were conducted using CasaXPS software. Raman spectroscopy measurements of MXene solutions were carried out using a Jasco NS-3100 Raman Spectrometer equipped with a 785 nm laser as the excitation source.

The electrical conductivity of all MXene film samples was measured in ambient conditions using the four-point probe on a Hall effect measurement system (ECOPIA, HMS-5500).

RESULTS AND DISCUSSION

MXene Nanosheet Properties. Figure 1a depicts the synthetic route used to form ${\rm Ti_3C_2T_x}$ MXene nanosheets from a MAX phase, which is etched using an acidic mixture of hydrofluoric/hydrochloric acid (HF/HCl) and delaminated using lithium chloride salt following a previously described protocol. Our characterization measurements of the resulting MXene nanosheets are in agreement with previous studies and indicate the formation of high-quality MXene nanosheets. The obtained greenish colloidal aqueous dispersions are highly stable in storage for over 6 months. The high stability of MXene nanosheet dispersions in water is attributed to the presence of high-alumina content in the precursor MAX phase. Earlier studies have shown that high aluminum content in the

ACS Applied Nano Materials www.acsanm.org

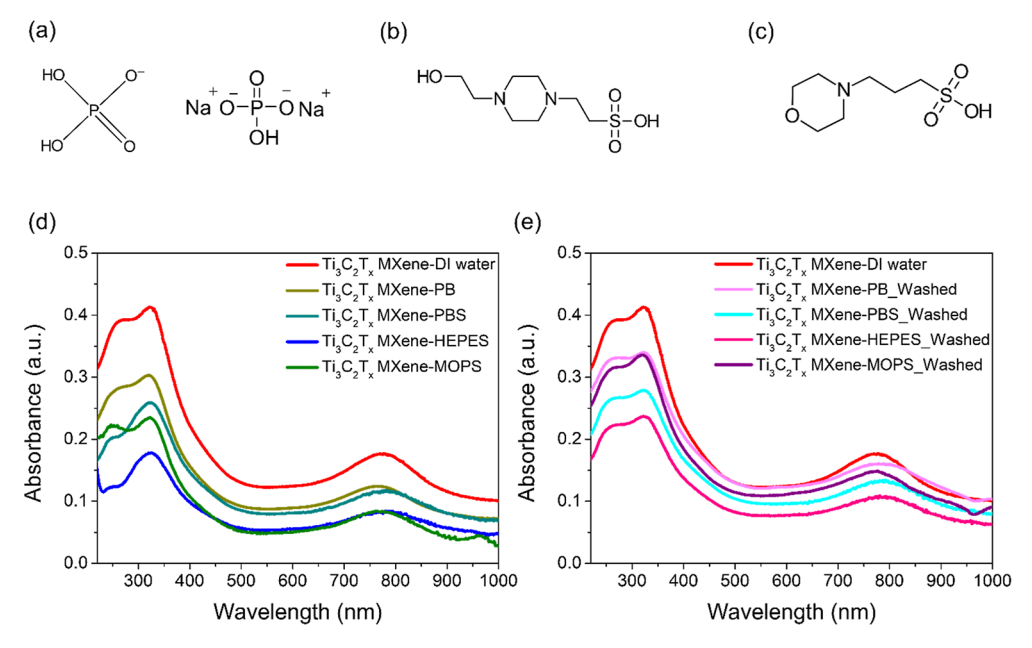


Figure 2. (a–c) Molecular structures of buffers: (a) phosphate, (b) HEPES, and (c) MOPS; (d–e) UV–vis spectra of $Ti_3C_2T_x$ MXene (d) dispersed in Deionized (DI) water and 10 mM PB, PBS, HEPES, and MOPS buffers, at a pH of 7.2, and (e) washed with DI water to remove buffer ions and molecules.

Ti₃AlC₂ MAX phase precursor results in the formation of Ti₃AlC₂ grains with improved crystallinity and carbon stoichiometry, which in turn leads to enhanced chemical and colloidal stability.⁵¹ The stable aqueous MXene dispersions exhibit an easily observed Tyndall effect (Figure 1b), suggesting the presence of MXene monolayers. The presence of monolayers is also confirmed by TEM measurements (Figure 1c), which show MXene nanosheets with lateral dimensions in the micrometer range. Nanosheets of such large lateral dimensions were previously reported to exhibit higher chemical stability toward oxidation. The presence of dotted rings in the SAED pattern (Figure 1d) obtained using high-resolution TEM (HRTEM) measurements confirms the formation of highly crystalline MXene nanosheets. The XRD pattern presented in Figure 1e indicates the conversion of the MAX phase into MXene. The significant weakening of the 2θ peak at around ~39° indicates the removal of aluminum, ²⁶ while the small peak indicates the presence of a small fraction of residues of the Ti_3AlC_2 MAX phase. The low-angle 2θ shift of the (002) peak in the XRD pattern and the observed peak broadening also confirm the delamination of MXene nanosheets from the MAX phase. The increased d-spacing is attributed to the intercalation of water molecules between MXene nanosheets. 10,17,56

The UV-vis spectrum of the MXene nanosheet solution is shown in Figure 1f. Unlike the UV-vis spectrum of the MAX phase³⁴ that shows relatively flat spectrum from 200 to 1000 nm, the UV-vis spectrum of MXene shows prominent absorbances in the UV as well as visible region. The intensity and shape of the UV absorption peak at 300 nm correspond to surface terminations, flake size, and shape of the MXene nanosheets. The intensity and shape of the visible absorption peak at 765 nm are consistent with fully etched and highly delaminated MXene nanosheets. ^{1,34} The Raman spectrum of delaminated MXene nanosheets (Figure 1g) shows multiple Raman bands that are distinct from those of the Ti₃AlC₂ MAX phase.⁵¹ The occurrence of prominent peaks at 206 cm⁻¹ and in the region between 590 and 740 cm⁻¹, which are attributed

to out-of-plane vibrations of Ti and C atoms, also confirm the formation of highly delaminated ${\rm Ti_3C_2T_x}$ MXenes. The presence of prominent peaks at 290 and 368 cm⁻¹ indicate a high density of hydroxyl and other oxygen containing functional groups on the surface of the MXene nanosheets, which results in a highly hydrophilic surface. The hydrophilicity enables loading of MXene interlayer spaces with water molecules when the MXene nanosheets are suspended in aqueous solution, thereby increasing the interlayer spacing.

Article

UV-Vis Spectroscopy Studies of MXene Nanosheets in Aqueous Biological Buffers. Phosphate buffer (PB) and phosphate-buffered saline (PBS) and the zwitterionic buffers HEPES and MOPS (structures shown in Figure 2a-c) are used widely in biological research due to their high stability, aqueous solubility, and inertness. ^{58,59} HEPES and MOPS, which have low metal-binding constants, ⁶⁰ are buffers of choice for enzyme-related studies, where preserving metal ions is essential for maintaining enzyme activity. A layer of M₃C₂ MXene, such as Ti₃C₂T_x constituting a transition-metal carbide (Ti₃C₂) core, possesses a positive charge, while the surface functionalities (T_x) are negatively charged. Thus, the positively and negatively charged components of MXenes interact electrostatically with the oppositely charged domains of HEPES and MOPS buffers. Figure 2d shows the UV-vis spectra of Ti₃C₂T_x MXene nanosheets dispersed in DI water (MXene-DI water), 10 mM PB (MXene-PB), 10 mM PBS (MXene-PBS), 10 mM MOPS (MXene-MOPS), and 10 mM HEPES (MXene-HEPES) buffers at pH 7.2. The MXene nanosheet solutions show characteristic UV and visible absorption peaks.

Earlier studies revealed that the absorption peaks at 262 and 323 nm are signature absorption peaks of MXene nanosheets that depend on their flake size, shape, and surface terminations. The changes in the peaks observed in our study are not necessarily related to the change in flake size or shape but to the adsorption of buffer molecules on the surface of MXenes. Table 1 summarizes the ratios between the absorption intensities of MXene nanosheets at λ_{262nm} and

Table 1. Ratio of UV-Vis Absorption Intensities at 262 and 323 nm for DI Water and Various Buffer Solutions at pH 7.2

MXenes in	$I_{\lambda 262\mathrm{nm}}/I_{\lambda 323\mathrm{nm}}$	MXenes washed from	$I_{\lambda 262\mathrm{nm}}/I_{\lambda 323\mathrm{nm}}$
DI water	0.95	DI water	0.95
PB	0.93	PB	0.97
MOPS	0.93	MOPS	0.94
PBS	0.78	PBS	0.95
HEPES	0.67	HEPES	0.94

 $\lambda_{323\text{nm}} (I_{262\text{nm}}/I_{323\text{nm}})$ when suspended in DI water and 10 mM PB, PBS, MOPS, and HEPES buffer solutions. The ratio $I_{\lambda_{262mp}}$ $I_{\lambda_{323nm}}$ provides an estimate of the degree of adsorption of buffer molecules on MXenes. Minimal or no effect on $I_{\lambda_{262\mathrm{nm}}}/I_{\lambda_{323\mathrm{nm}}}$ is observed when MXene nanosheets are incubated in DI water and phosphate and MOPS buffers at pH 7.2. On the other hand, suspending MXene nanosheets in PBS (MXene-PBS) leads to a noticeable decrease in the absorption intensity of MXene nanosheets in the UV region and to a large change in $I_{262\text{nm}}/I_{323\text{nm}}$ (shown in bold in Table 1), which indicates strong interactions of MXene nanosheets with Na⁺ ions that adsorb onto the MXene surface and intercalate between MXene layers.⁶⁴ Even stronger interactions are observed when MXene nanosheets are suspended in HEPES, where the UVvis spectrum shows a significant decrease in absorption in both the UV and visible absorption peaks. The strong absorption peak at around 235 nm and the weak absorption peak at around 660 nm are attributed to the complexation of HEPES molecules with MXene nanosheets. While HEPES buffer molecules are chemically stable and do not tend to form complexes with biological molecules and materials, the formation of complexes between HEPES molecules and transition-metal ions in aqueous solution, for example Cu(II)-HEPES complexes has been observed.⁶⁰ It is noteworthy that despite the MXene-HEPES complexation, no

precipitation or aggregation of MXene nanosheets is observed. The interactions of HEPES molecules with MXenes are concentration-dependent (Figure S1). The strong interactions of MXene nanosheets with HEPES molecules could be explained by the formation of coordination bonds between hydroxyl and tertiary amine groups in HEPES and the Ti atoms in the MXene nanosheets. This, in turn, leads to the formation of a chelate ring on the MXene surface. Our UV—vis results also show a recovery of the spectral features of MXene nanosheets including $I_{262 \mathrm{nm}}/I_{323 \mathrm{nm}}$ when washed extensively with DI water to remove the sodium ions and HEPES molecules, but the large changes in the spectral features of MXene nanosheets in PBS and HEPES buffers raised concerns about the impact of these exposures on MXenes' functional properties.

To determine whether the interactions of MXene nanosheets with various buffer molecules permanently affect MXene structural and electronic properties, the MXene nanosheets were suspended in various buffer solutions for 8 days, then washed three times, and redispersed in DI water. A significant irreversible red shift from 774 to 794 nm in the UV-vis spectrum of MXene nanosheets following their longer incubation with HEPES molecules was observed (Figure 2e). This suggests a certain degree of chemisorption of HEPES molecules that either remain bound to the MXene nanosheets even after excessive washing or lead to permanent damage, possibly due to surface oxidation. A similar phenomenon, albeit to a lesser extent, was observed in MXene-MOPS solutions. The lower decrease in absorption peak intensities in MXene-MOPS suggests weaker interactions between the MOPS molecules and the MXene nanosheets, most likely due to the absence of donor atoms on the α -, β -, or γ -carbons of the morpholine ring. The differences in the strength of interaction between MXene-HEPES and MXene-MOPS might be attributed to the higher electron-donating ability of the piperazine ring of HEPES than the electron-donating ability of the morpholine ring of MOPS molecules. XRD and

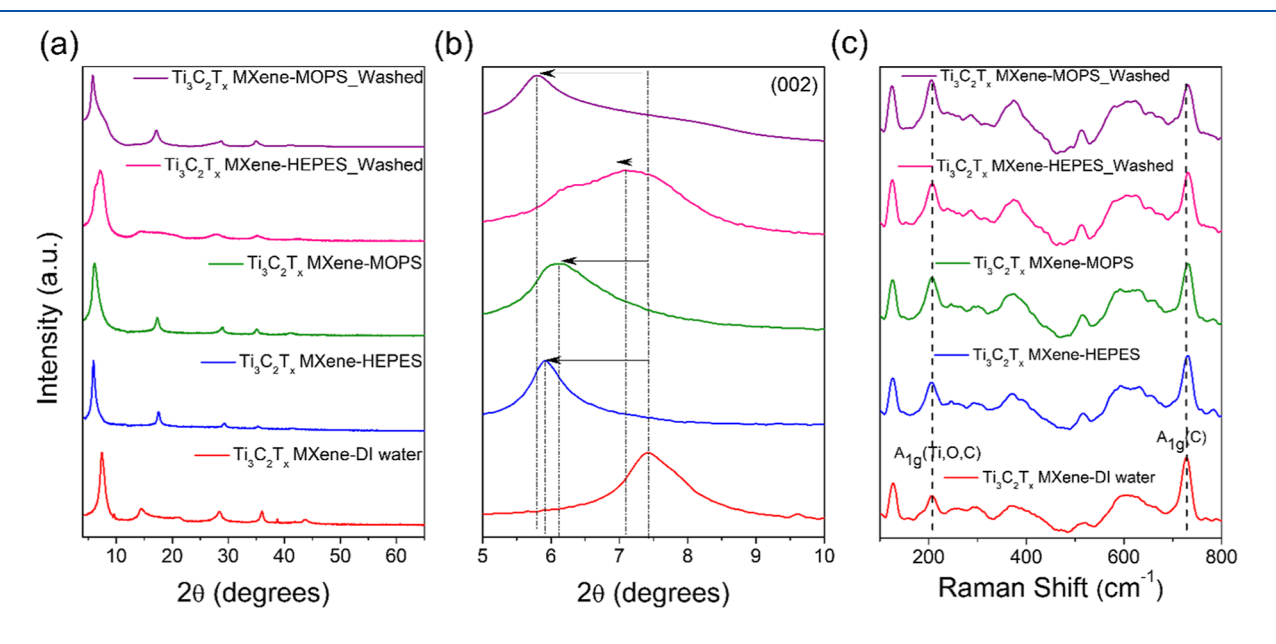


Figure 3. (a) XRD patterns of MXene nanosheets in DI water (MXene–DI water, red), 10 mM HEPES buffer (MXene–HEPES, blue), 10 mM MOPS buffer (MXene@MOPS, green), a washed sample of MXene nanosheets from HEPES (MXene–HEPES washed, pink), and a washed sample of MXene nanosheets from MOPS (MXene–MOPS washed, purple), (b) magnified XRD patterns of the (002) 2θ region of all five samples, and (c) Raman spectra of the five samples.

ACS Applied Nano Materials

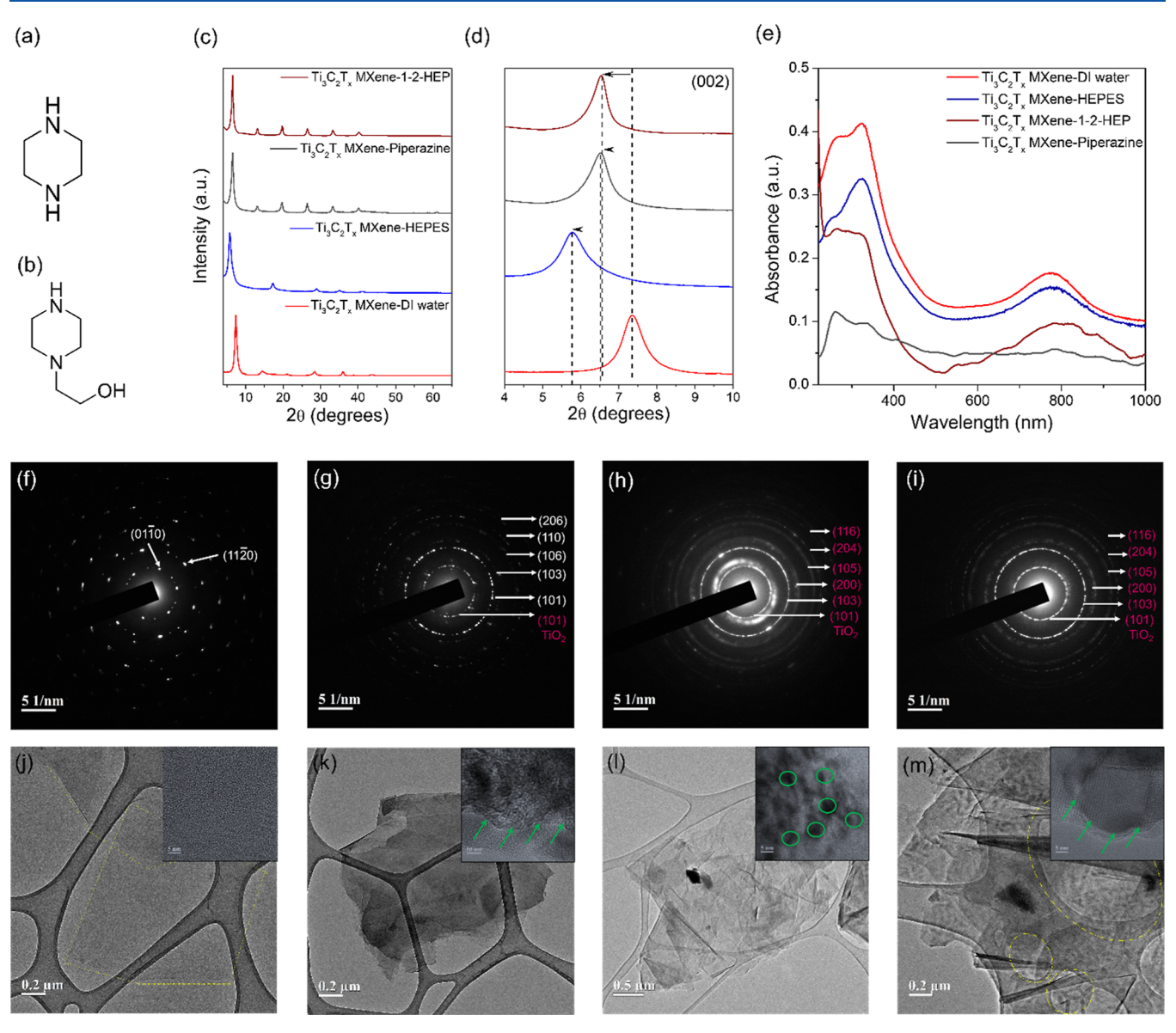


Figure 4. Molecular structures of analogues of HEPES: (a) piperazine, (b) 1-2-HEP, (c) XRD pattern, and (d) magnified XRD patterns of the (002) 2θ region. (e) UV-vis spectra of MXenes in all analogues of HEPES, SAED patterns of (f) MXene-DI water, (g) MXene-HEPES, (h) MXene-1-2-HEP, and (i) MXene-Piperazine. TEM images of (j) MXene-DI water, (k) MXene-HEPES, (l) MXene-1-2-HEP, and (m) MXene-Piperazine, the inset of (j-m): HRTEM images. These analyses discuss the impact of interactions of MXenes with HEPES and its analogues on the structure of MXenes.

Raman measurements were used to further investigate the interactions between HEPES and MOPS molecules and MXene nanosheets.

XRD and Raman Studies of MXene Nanosheets in HEPES and MOPS Buffer Solutions. XRD measurements used to confirm and compare the intercalation efficiency of HEPES and MOPS molecules into layered MXene nanosheets are shown in Figure 3. Figure 3a shows the XRD patterns of MXene nanosheets in DI water (MXene–DI water, red), 10 mM HEPES buffer at pH 7.2 (MXene–HEPES, blue), 10 mM MOPS buffer at pH 7.2 (MXene–MOPS, green), and MXene nanosheets, which were washed multiple times to remove HEPES (pink) and MOPS (purple) buffer molecules. Figure 3b highlights the low-angle 2θ region range of $5-10^\circ$, which corresponds to the (002) peak, a characteristic peak of the c-lattice parameter of MXene nanosheets. As is seen, the peaks corresponding to the basal direction are relatively broad. We

ascribe them to the relatively improved in-plane alignment of flakes in the buffer-intercalated films. The c-lattice parameter either expands or contracts under various circumstances, such as the intercalation of water molecules, organic molecules, and ions in between MXene layers or the functionalization of MXene nanosheets with surface ligands. 17,39,64 The distance between monolayers, defined as the d-spacing, is calculated from the XRD patterns. The dspacing provides important information about the intercalation of HEPES and MOPS molecules between MXene monolayers. For MXenes, the d-spacing is calculated by dividing the clattice parameter by 2.65 The d-spacing of MXene nanosheets in DI water is 12.05 \pm 0.01 Å. It increases to 15.30 \pm 0.01 and 15.44 ± 0.01 Å in MXene-HEPES and MXene-MOPS, respectively. Being hydrophilic, the 2D structure of MXene easily accommodates the HEPES and MOPS molecules, thereby expanding the basal spacing. The increase in *d*-spacing

induced by HEPES and MOPS molecules is similar. The dspacing values decrease from 15.44 \pm 0.01 to 15.32 \pm 0.01 Å when MXene-MOPS nanosheets are washed and from 15.30 \pm 0.01 to 14.63 \pm 0.01 Å, on washing MXene-HEPES nanosheets. The notable appearance of the second (002) shoulder peak in the MXene-HEPES washed sample at 6.28° (Figure 3b, pink diffractogram) indicates the presence of intercalated guest species (HEPES), creating a large interlayer space between two adjacent nanosheets. 66 In both cases, the dspacing values remain far off the d-spacing value of MXene in DI water (12.05 \pm 0.01 Å). Most importantly, the retention of high d-spacing values in MXene-HEPES and MXene-MOPS after washing compared to the *d*-spacing value of MXene–DI water despite repeated washing cycles strongly supports our interpretation of the UV-vis measurements (Figure 2) that some HEPES and MOPS molecules intercalate and remain trapped in the MXene nanosheets despite multiple washing cycles. These measurements also suggest that the presence of HEPES or MOPS molecules between MXene layers is not sufficient to induce a change in functional properties. Such changes depend on the strength and nature of interactions of the adsorbates with the MXene surface.

Raman spectroscopy studies were carried out to gain a greater molecular understanding of the interactions between MXene nanosheets and HEPES and MOPS molecules and their impact on the morphology and order of the nanosheets. The Raman spectra of MXene-HEPES and MXene-MOPS solutions before and after washing are presented in Figure 3c. Being stiffest, the out-of-plane vibrations of the titanium carbide core [A_{1g}(Ti,O,C)] remain unchanged. Sarycheva and Gogotsi ascribed this to the presence of the maximum number of atoms occupying the MXene unit cell. However, peak shifts are observed in the out-of-plane vibrations corresponding to carbon atoms $[A_{1g}(C)]$, suggesting differences in intercalation. The shifts in A_{1g}(C) from 727 cm⁻¹ in MXenes-DI water to 730 cm⁻¹ in MXene-HEPES and 731 cm⁻¹ in MXene-MOPS are consistent with the increase in interlayer spacing.⁵⁷ Moreover, the differences in the intensities of A_{lg} (C) in all samples reveal that the vibrations of the carbon layer depend on the nanosheets' orientation. The ratio of $A_{1g}(C)$ / $A_{1g}(Ti,O,C)$ gives a quantitative estimate of the orientation of MXene nanosheets and their interactions with buffer molecules. The ratio $A_{1g}(C)/A_{1g}(Ti,O,C)$ of MXene–DI water is 2.78. This high $A_{1g}(C)/A_{1g}(Ti,O,C)$ value indicates that when suspended in DI water, our delaminated MXenes are mostly monolayers with a high degree of freedom in terms of nanosheet orientation. The ratio $A_{1g}(C)/A_{1g}(Ti,O,C)$ decreases to 1.94 and 1.30 in MXene-HEPES and MXene-MOPS, respectively. As HEPES or MOPS molecules intercalate between MXene monolayers and increase the dspacing, they also appear to form a more ordered layer-by-layer structure where multiple MXene nanosheets are held together by the intercalating HEPES or MOPS molecules. When the MXene nanosheets are washed and resuspended in DI water, most but not all HEPES or MOPS molecules are removed. Furthermore, the $A_{1g}(C)/A_{1g}(Ti,O,C)$ values of the MXene nanosheets further decrease when washed of HEPES $[A_{1g}(C)]$ $A_{1g}(Ti,O,C)$ value of 1.29] and of MOPS $[A_{1g}(C)/$ $A_{1g}(Ti,O,C)$ value of 1.12]. The differences in the $A_{1g}(C)$ A_{1g}(Ti,O,C) values of MXene-HEPES and MXene-MOPS indicate that the orientation of MXene layers is different in the layer-by-layer structures formed in HEPES or MOPS buffer solutions. Nevertheless, the formed MXene intercalated

structures remain stable and aggregation free in both buffers and even after washing.

Interactions of MXene Nanosheets with HEPES **Derivatives.** To understand the role of hydroxyl and sulfonyl groups in the interactions of HEPES molecules with MXene nanosheets, we carried out experiments with the HEPES analogues piperazine that does not contain hydroxyl and sulfonyl groups (Figure 4a) and (1-2-(hydroxyethyl) piperazine) (1-2-HEP) that contains a hydroxyl but no sulfonyl group (Figure 4b). Figure 4c presents the XRD patterns of MXene-HEPES, MXene-Piperazine, and MXene-1-2-HEP. The low-angle 2θ region ranging from 5 to 10° , which corresponds to the (002) peak, is presented in Figure 4d. Lowangle 2θ shifts in the XRD patterns of MXene nanosheets indicate the intercalation of HEPES and its two analogues in between monolayers of MXenes. Figure 4e shows the UV-vis absorption spectra of MXene-HEPES, MXene-Piperazine, and MXene-1-2-HEP solutions, all at 2 mM concentration and pH 7.2. The UV-vis spectra of the MXene-HEPES (blue), MXene-Piperazine (gray), and MXene-1-2-HEP (brown) preserve the main spectral features seen in the UV-vis spectrum of MXene-DI water (red). However, the absorption intensity decrease is much more significant in MXene-1-2-HEP, indicating stronger interactions of 1-2-HEP with MXene nanosheets. The absence of the sulfonyl group in 1-2-HEP decreases the molecule size compared to HEPES, lowers its hydrophilicity, increases its intercalation efficiency, and decreases the rate of release of 1-2-HEP to the solution following washing. It is noteworthy that the MXene nanosheets remain stable and aggregation free in both HEPES and 1-2-HEP solutions, most likely due to the presence of hydroxyl groups in both molecules. In contrast, molecules like piperazine that do not contain hydroxyl or sulfonyl groups rapidly aggregate MXene nanosheets. This is evident from a lower signal-to-noise ratio, probably due to increased light scattering in the UV-vis spectrum of MXene nanosheets in piperazine solution (Figure 4e).

To elucidate the structural changes on MXene nanosheets, we measured the SAED patterns of MXenes after exposure to the different solutions. The SAED pattern of MXene–DI water (Figure 4f) is a signature pattern assigned to the hexagonal symmetry of crystalline Ti₃C₂ MXenes. The SAED patterns presented in Figure 4g-i reveal the formation of a ring, typically observed when an anatase phase of TiO2 is present, indicating the onset of surface oxidation of the MXene nanosheets. A comparison of the SAED patterns of MXene-HEPES (Figure 4g), MXene-1-2-HEP (Figure 4h), and MXene-Piperazine (Figure 4i) shows that the severity of oxidation follows MXene-HEPES < MXene-1-2-HEP < MXene-Piperazine. The presence of hydroxyl and sulfonyl groups in HEPES and hydroxyl groups in 1-2 HEP decreases the MXene nanosheets' oxidation rate due to increased hydrophilicity but does not prevent it. TEM measurements were also used to determine the structural impact of HEPES and its analogues on MXene nanosheets (Figure 4j-m). Figure 4j shows the TEM image of stable MXene-DI water that is free of oxidation or any degradation even when suspended in DI water for several months. In contrast to the planar and smooth surface of MXene flakes in DI water (Figure 4j), the presence of dark nucleated regions seen in TEM images of MXene-HEPES (Figure 4k), MXene-1-2-HEP (Figure 4l), and MXene-Piperazine (Figure 4m) indicate the presence of these organic molecules on the surface of MXenes. These

ACS Applied Nano Materials

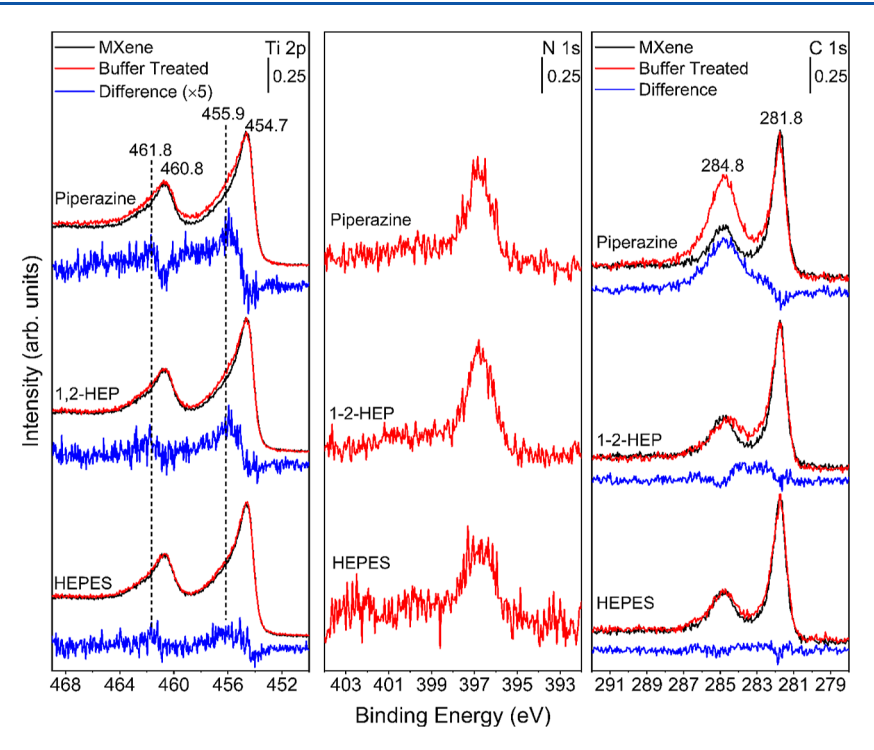


Figure 5. Elemental XPS spectra (a) Ti 2p, (b) N 1s, and (c) C 1s of Ti₃C₂T_x MXenes in DI water (black curves), HEPES, 1,2-HEP, and piperazine molecules. The XPS spectra provide evidence of the oxidation of MXenes on their interaction with HEPES and HEPES analogues.

effects are observed in the HRTEM images shown as insets in Figure 4j—m. When exposed to insoluble piperazine molecules with no hydroxyl and sulfonyl groups, the MXene nanosheets aggregate, which leads to the formation of pinholes or defects on the surface of the MXene nanosheets (Figure 4m). The presence of defects is also evident from the formation of large sphere-like particles (inset of Figure 4m) on the surface of MXenes.

XPS measurements were carried out to better understand the adsorbate-MXene interactions along with the parameters affecting surface oxidation of MXene nanosheets in solutions of HEPES and its derivatives. XPS survey spectra (Figure S2) of MXene samples in DI water (MXene), HEPES (MXene-HEPES), 1-2-HEP (MXene-1-2-HEP), and piperazine (MXene-Piperazine) show the constituent elements of the participating species in each sample. In general, the interactions of HEPES and its derivatives do not produce large or significant changes in the XPS data, as evidenced by the similarity of all the survey spectra (0-1000 eV) shown in Figure S2. This suggests that the overall degree of buffer adsorption to the MXene surface is relatively small and/or the strength of adsorbate-substrate bonding is not sufficiently strong to allow most of the buffer molecules to remain adsorbed under UHV conditions. However, closer inspection of the Ti 2p, N 1s, and C 1s transitions shown in Figure 5a-c does reveal subtle changes. The XPS spectra of MXene nanosheets in DI water and HEPES, 1-2-HEP, and piperazine are shown in black (prior to washing) and red (following washing). The difference spectra between the unwashed and washed MXene nanosheets are shown in blue. As a result of atomic-spin orbit interactions, the Ti 2p region in Figure 5a is composed of $2p_{3/2}$ and $2p_{1/2}$ peaks at 455.9 and 461.8 eV, respectively. As observed in Figure 5a, peaks at 455.9 and 461.8 eV in the blue spectra correspond to the oxidation of Ti, most likely in the form of TiO₂. The oxidation is most

pronounced when the MXene nanosheets are treated with piperazine and least when treated with HEPES, which correlates with the pK_a of the buffer. On washing MXene-HEPES, the oxidized peaks, presumably associated with the asformed TiO2, get washed away, as evidenced by the absence of any spectral intensity in the difference spectra of the Ti 2p region of MXene-HEPES washed (Figure S3a) compared to the native MXene. Analogous results regarding the removal of oxidized Ti species were observed for MXenes treated in MOPS buffer and then washed. In the Ti 2p regions of MXene-1-2-HEP and MXene-Piperazine, the extent of Tioxidation increases compared to MXene-HEPES (Figure 5a), an indication of the greater degree of TiO2. The N 1s spectra of all samples are presented in Figure 5b. The N 1s spectrum of MXene in DI water shows no intensity contributions from nitrogen, while contributions from nitrogen are seen in MXene-HEPES and MXene-1-2-HEP and MXene-Piperazine, indicative of adsorption. The more significant adsorption in MXene-1-2-HEP and MXene-Piperazine is ascribed to the structural differences in the organic molecules interacting with MXenes. Figure 5c shows the C1s spectra of all the samples subtracted from that of MXenes. All samples have observed no appreciable change in the carbide region (Ti-C) at around 282.0 eV. This indicates no hindrance to the carbide core region when zwitterionic buffers and their analogues interact with MXenes. However, exciting trends in the adventitious carbon region (284.8 eV) are observed. The zwitterionic HEPES and MOPS (Figure S3b) both appear to remove a significant fraction of the adventitious carbon from the layers of MXenes. This observation could be helpful in terms of pretreating MXenes for subsequent surface functionalization as adventitious carbon blocks otherwise active surface sites such as Ti-OH groups. In contrast, the adventitious carbon increases when MXenes interact with piperazine (Figure 5c).

ACS Applied Nano Materials

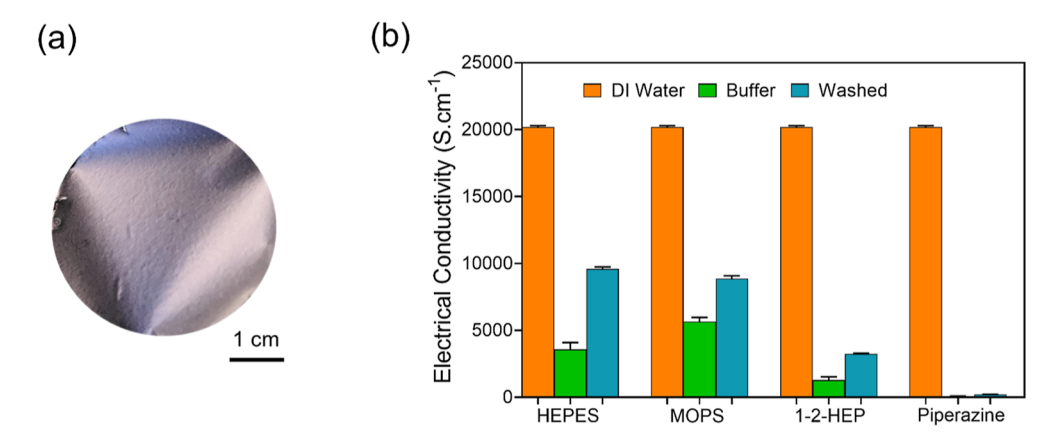


Figure 6. (a) Photograph of the Ti_3C_2 MXene film (about 5 μ m thick) obtained by vacuum filtration of colloidal MXene solution, and (b) electrical conductivity of MXenes in DI water, buffer suspensions, and when washed. The MXene properties are clearly affected when MXene interacts with different organic molecules.

ı

Effect of MXene Interactions with HEPES, MOPS, and Their Analogues on the Electrical Conductivity. The previous sections provided clear evidence for a significant and partially irreversible impact of HEPES, MOPS, and their molecular analogues on MXene nanosheets. We also determined whether the interactions of MXenes with zwitterionic buffers HEPES and MOPS and the analogues of HEPES affect the conductivity of MXene films. These measurements are critical since MXene nanosheets are often used as components in electrical devices due to their excellent conductivity properties. Thin films of MXenes were obtained by vacuum filtering colloidal solutions of MXene nanosheets, which were dispersed in HEPES, MOPS, or HEPES analogue solutions. The representative photograph of the free-standing Ti₃C₂T_x MXene film is shown in Figure 6a. Such free-standing films were used to measure electrical conductivity. All films were dried and annealed under the same conditions prior to conductivity measurements, which were carried out using a four-point probe. The measured conductivity of MXene films prepared from DI water (orange bars) was 20,200 S cm⁻¹. Figure 6b shows that the conductivity of films prepared from MXene-HEPES and MXene-MOPS (green bars) decreases to 4171 and 5908 S cm⁻¹, respectively. The conductivity significantly decreases with MXene interactions in 1-2-HEP (1540 S cm⁻¹) and piperazine (95 S cm⁻¹). These results suggest that the intercalation and inability to completely wash molecular species blocks contact points between MXene nanosheets, which leads to a significant decrease in the electrical conductivity of MXene films in these solutions. In the case of interactions with HEPES analogues 1-2-HEP and piperazine, such a drastic loss in conductivity is attributed to the formation of anatase TiO2 and structural defects in the MXenes. A much higher loss in conductivity in MXene-Piperazine (95 cm⁻¹) compared to MXene-1-2-HEP (1540 cm⁻¹) results from greater TiO₂ formation and suggests the formation of defects on MXene flakes. To determine the degree of reversibility of the impact of HEPES, MOPS, and HEPES analogues on the conductivity of MXene films, the MXene films were thoroughly washed, resuspended in DI water, and vacuum filtered to obtain free-standing MXene films. As seen in Figure 6b, washing an MXene film derived from MXene-HEPES more than doubled the MXene film's conductivity, increasing from 4171 to 9760 S cm⁻¹. Similarly, washing an MXene film derived from MXene-MOPS

increased the MXene film's conductivity by 1.5 folds from 5908 to 9100 S cm⁻¹. The increased conductivity of both films by washing suggests the removal of HEPES and MOPS that were weakly bound to the MXene films. In contrast, the conductivity of MXene films derived from MXene-1-2-HEP and MXene-Piperazine solutions increased only slightly following washing, indicating more permanent damage caused by MXene film oxidation and/or defect formation. It should be noted that in all MXene films, which were derived from HEPES, MOPS, or HEPES analogues, the electrical conductivity of the films was not fully restored following washing. The negative impact on MXene films' conductivity due to exposure to these organic molecules is significant and irreversible, even if only a small number of molecules remain attached or entrapped between MXene layers, as suggested by the XPS data.

CONCLUSIONS

MXenes have gained increasing attention and popularity as components of electronic and energy conversion devices. Recently, they have also been proposed for numerous applications in aqueous media including but not limited to water treatment and biomedical devices that involve their exposure to complex biological solutions. Such complex aqueous environments pose a challenge. While the availability of active surface functional groups like hydroxyl and fluoride provides anchoring sites for surface conjugation and intercalation of molecules into the MXene layered structure, these same functional groups and MXene hydrophilicity make MXenes vulnerable to destructive interactions with chemical constituents in complex biological solutions. The interactions between MXenes and common aqueous solution constituents must be better understood for successful application of MXenes in complex biological solutions. Our study shows that the interactions of N-containing buffer molecules like HEPES and HEPES derivatives and MXene nanosheets lead to their intercalation and disruption of the MXene layered structure. UV-vis results show significant changes in the absorption spectra including an overall decrease in absorption and changes in the ratio between UV peaks when MXene nanosheets are exposed to these molecules and to sodium ions in aqueous solution. Our UV-vis results also show the recovery of most absorption features of MXene nanosheets when washed extensively and suspended in DI water. However,

our XRD, XPS, and conductivity measurements show a nonreversible impact on MXene nanosheets due to these exposures, which in some cases lead to surface oxidation and permanent degradation of functional properties, most importantly MXene nanosheets' conductivity. The sulfonyl groups of HEPES and MOPS buffers play an essential role in controlling the rate of oxidation of the 2D Ti₃C₂ network. It should be noted that many biomolecules have similar molecular motifs to HEPES and HEPES derivatives and interactions of similar or even higher strength of biomolecules with MXenes are expected. The increasing strength of interactions with the increase in hydrophobic characters suggests that biomolecules with hydrophobic domains like lipids would interact more strongly with MXene surfaces. This study is an important step toward understanding the behavior of MXene nanosheets in biological media. It reveals that ubiquitous adsorbates in biological solutions like HEPES and HEPES derivatives significantly impact the structural and functional properties of MXenes and that the strength of the effect is adsorbate structure-dependent. Further detailed studies of interactions of nitrogen-containing biomolecules with MXene surfaces to reveal whether the interactions are driven by surface defects and edge sites or by substitution of functional groups on MXene surfaces along with improving the stability and limiting the interactions of nitrogen-containing hydrophobic biomolecules with MXenes through directed surface modifications are necessary to preserve the structural and functional properties of MXenes and enable their successful applications in complex biological media.

ASSOCIATED CONTENT

Solution Supporting Information

The Supporting Information is available free of charge at https://pubs.acs.org/doi/10.1021/acsanm.3c00666.

UV—vis spectra of the concentration dependence of interactions of the HEPES buffer with MXene nanosheets; comparison of XPS survey spectra of MXenes in zwitterionic buffers and analogues of HEPES; and elemental XPS spectra of ${\rm Ti}_3{\rm C}_2{\rm T}_x$ MXenes washed in MOPS, HEPES, and MOPS (PDF)

AUTHOR INFORMATION

Corresponding Author

Zeev Rosenzweig — Department of Chemistry and Biochemistry, University of Maryland Baltimore County, Baltimore, Maryland 21250, United States; oorcid.org/ 0000-0001-6098-3932; Email: zrosenzw@umbc.edu

Authors

Swapnil B. Ambade – Department of Chemistry and Biochemistry, University of Maryland Baltimore County, Baltimore, Maryland 21250, United States

Laura A. Kesner – Department of Chemistry and Biochemistry, University of Maryland Baltimore County, Baltimore, Maryland 21250, United States

Mohammed K. Abdel-Rahman — Department of Chemistry, Johns Hopkins University, Baltimore, Maryland 21218-2685, United States; occid.org/0000-0002-8028-5258

D. Howard Fairbrother – Department of Chemistry, Johns Hopkins University, Baltimore, Maryland 21218-2685, United States; orcid.org/0000-0003-4405-9728

Complete contact information is available at:

https://pubs.acs.org/10.1021/acsanm.3c00666

Author Contributions

The manuscript was written through contributions of all authors as follows: S.B.A.—carried out the MXene synthesis and characterization studies and participated in writing this manuscript, L.A.K.—contributed to experiments of MXenes with biological buffers. M.K.A.-R.—assisted in XPS analysis and data interpretation of MXene nanosheets. D.H.F.—assisted in XPS analysis and data interpretation of MXene nanosheets. Z.R.—designed the study and served as the corresponding author. All authors have given approval to the final version of the manuscript.

Notes

The authors declare no competing financial interest.

ACKNOWLEDGMENTS

This study was supported by the National Science Foundation under grant no. CHE-2001611, which supports the NSF Center for Sustainable Nanotechnology (CSN). The authors are thankful to Christopher Shuck and Yury Gogotsi of Drexel University for providing the MAX phase material. The authors are grateful to Erina Kagami, Rigaku Americas Corporation, for carrying out XRD measurements of our MXene samples.

REFERENCES

- (1) VahidMohammadi, A.; Rosen, J.; Gogotsi, Y. The world of two-dimensional carbides and nitrides (MXenes). *Science* **2021**, *372*, 6547. (2) Gogotsi, Y.; Anasori, B. The Rise of MXenes. *ACS Nano* **2019**, *13*, 8491–8494.
- (3) Akuzum, B.; Maleski, K.; Anasori, B.; Lelyukh, P.; Alvarez, N. J.; Kumbur, E. C.; Gogotsi, Y. Rheological Characteristics of 2D Titanium Carbide (MXene) Dispersions: A Guide for Processing MXenes. ACS Nano 2018, 12, 2685–2694.
- (4) Pan, J.; Lany, S.; Qi, Y. Computationally Driven Two-Dimensional Materials Design: What Is Next? *ACS Nano* **2017**, *11*, 7560–7564.
- (5) Naguib, M.; Mashtalir, O.; Carle, J.; Presser, V.; Lu, J.; Hultman, L.; Gogotsi, Y.; Barsoum, M. W. Two-dimensional transition metal carbides. *ACS Nano* **2012**, *6*, 1322–1331.
- (6) Ghidiu, M.; Naguib, M.; Shi, C.; Mashtalir, O.; Pan, L. M.; Zhang, B.; Yang, J.; Gogotsi, Y.; Billinge, S. J.; Barsoum, M. W. Synthesis and characterization of two-dimensional Nb4C3 (MXene). *Chem. Commun.* **2014**, *50*, 9517–9520.
- (7) Khazaei, M.; Arai, M.; Sasaki, T.; Estili, M.; Sakka, Y. Two-dimensional molybdenum carbides: potential thermoelectric materials of the MXene family. *Phys. Chem. Chem. Phys.* **2014**, *16*, 7841–7849.
- (8) Naguib, M.; Mochalin, V. N.; Barsoum, M. W.; Gogotsi, Y. 25th anniversary article: MXenes: a new family of two-dimensional materials. *Adv. Mater.* **2014**, *26*, 992–1005.
- (9) Anasori, B.; Xie, Y.; Beidaghi, M.; Lu, J.; Hosler, B. C.; Hultman, L.; Kent, P. R.; Gogotsi, Y.; Barsoum, M. W. Two-Dimensional, Ordered, Double Transition Metals Carbides (MXenes). *ACS Nano* **2015**, *9*, 9507–9516.
- (10) Naguib, M.; Unocic, R. R.; Armstrong, B. L.; Nanda, J. Large-scale delamination of multi-layers transition metal carbides and carbonitrides "MXenes". *Dalton Trans.* **2015**, *44*, 9353–9358.
- (11) Urbankowski, P.; Anasori, B.; Makaryan, T.; Er, D.; Kota, S.; Walsh, P. L.; Zhao, M.; Shenoy, V. B.; Barsoum, M. W.; Gogotsi, Y. Synthesis of two-dimensional titanium nitride Ti4N3 (MXene). *Nanoscale* **2016**, *8*, 11385–11391.
- (12) Zhou, J.; Zha, X.; Chen, F. Y.; Ye, Q.; Eklund, P.; Du, S.; Huang, Q. A Two-Dimensional Zirconium Carbide by Selective Etching of Al3C3 from Nanolaminated Zr3Al3C5. *Angew. Chem., Int. Ed. Engl.* **2016**, *55*, 5008–5013.

- (13) Soundiraraju, B.; George, B. K. Two-Dimensional Titanium Nitride (Ti2N) MXene: Synthesis, Characterization, and Potential Application as Surface-Enhanced Raman Scattering Substrate. *ACS Nano* **2017**, *11*, 8892–8900.
- (14) Urbankowski, P.; Anasori, B.; Hantanasirisakul, K.; Yang, L.; Zhang, L.; Haines, B.; May, S. J.; Billinge, S. J. L.; Gogotsi, Y. 2D molybdenum and vanadium nitrides synthesized by ammoniation of 2D transition metal carbides (MXenes). *Nanoscale* **2017**, *9*, 17722–17730.
- (15) Zhou, J.; Zha, X.; Zhou, X.; Chen, F.; Gao, G.; Wang, S.; Shen, C.; Chen, T.; Zhi, C.; Eklund, P.; Du, S.; Xue, J.; Shi, W.; Chai, Z.; Huang, Q. Synthesis and Electrochemical Properties of Two-Dimensional Hafnium Carbide. *ACS Nano* **2017**, *11*, 3841–3850.
- (16) Magne, D.; Mauchamp, V.; Célérier, S.; Chartier, P.; Cabioc'h, T. Site-projected electronic structure of two-dimensional Ti3C2 MXene: the role of the surface functionalization groups. *Phys. Chem. Chem. Phys.* **2016**, *18*, 30946–30953.
- (17) Mashtalir, O.; Naguib, M.; Mochalin, V. N.; Dall'Agnese, Y.; Heon, M.; Barsoum, M. W.; Gogotsi, Y. Intercalation and delamination of layered carbides and carbonitrides. *Nat. Commun.* **2013**, *4*, 1716.
- (18) Xie, Y.; Dall'Agnese, Y.; Naguib, M.; Gogotsi, Y.; Barsoum, M. W.; Zhuang, H. L.; Kent, P. R. Prediction and characterization of MXene nanosheet anodes for non-lithium-ion batteries. *ACS Nano* **2014**, *8*, 9606–9615.
- (19) Zhan, C.; Sun, W.; Xie, Y.; Jiang, D. E.; Kent, P. R. C. Computational Discovery and Design of MXenes for Energy Applications: Status, Successes, and Opportunities. *ACS Appl. Mater. Interfaces* **2019**, *11*, 24885–24905.
- (20) Pang, J.; Mendes, R. G.; Bachmatiuk, A.; Zhao, L.; Ta, H. Q.; Gemming, T.; Liu, H.; Liu, Z.; Rummeli, M. H. Applications of 2D MXenes in energy conversion and storage systems. *Chem. Soc. Rev.* **2019**, *48*, 72–133.
- (21) Shang, M.; Chen, X.; Li, B.; Niu, J. A Fast Charge/Discharge and Wide-Temperature Battery with a Germanium Oxide Layer on a Ti3C2 MXene Matrix as Anode. ACS Nano 2020, 14, 3678–3686.
- (22) Ambade, S. B.; Ambade, R. B.; Eom, W.; Noh, S. H.; Kim, S. H.; Han, T. H. 2D Ti3C2 MXene/WO3 Hybrid Architectures for High-Rate Supercapacitors. *Adv. Mater. Interfac.* **2018**, *5*, 1801361.
- (23) Rakhi, R. B.; Nayak, P.; Xia, C.; Alshareef, H. N. Novel amperometric glucose biosensor based on MXene nanocomposite. *Sci. Rep.* **2016**, *6*, 36422.
- (24) Lee, E.; VahidMohammadi, A.; Prorok, B. C.; Yoon, Y. S.; Beidaghi, M.; Kim, D. J. Room Temperature Gas Sensing of Two-Dimensional Titanium Carbide (MXene). ACS Appl. Mater. Interfaces 2017, 9, 37184–37190.
- (25) Pang, D.; Alhabeb, M.; Mu, X.; Dall'Agnese, Y.; Gogotsi, Y.; Gao, Y. Electrochemical Actuators Based on Two-Dimensional Ti3C2Tx (MXene). *Nano Lett.* **2019**, *19*, 7443–7448.
- (26) Koh, H. J.; Kim, S. J.; Maleski, K.; Cho, S. Y.; Kim, Y. J.; Ahn, C. W.; Gogotsi, Y.; Jung, H. T. Enhanced Selectivity of MXene Gas Sensors through Metal Ion Intercalation: In Situ X-ray Diffraction Study. ACS Sens. 2019, 4, 1365–1372.
- (27) Zhu, D.; Liu, B.; Wei, G. Two-Dimensional Material-Based Colorimetric Biosensors: A Review. *Biosensors* **2021**, *11*, 259.
- (28) Lee, S. H.; Eom, W.; Shin, H.; Ambade, R. B.; Bang, J. H.; Kim, H. W.; Han, T. H. Room-Temperature, Highly Durable Ti3C2Tx MXene/Graphene Hybrid Fibers for NH3 Gas Sensing. ACS Appl. Mater. Interfaces 2020, 12, 10434–10442.
- (29) Eom, W.; Shin, H.; Ambade, R. B.; Lee, S. H.; Lee, K. H.; Kang, D. J.; Han, T. H. Large-scale wet-spinning of highly electroconductive MXene fibers. *Nat. Commun.* **2020**, *11*, 2825.
- (30) Shin, H.; Eom, W.; Lee, K. H.; Jeong, W.; Kang, D. J.; Han, T. H. Highly Electroconductive and Mechanically Strong Ti3C2Tx MXene Fibers Using a Deformable MXene Gel. *ACS Nano* **2021**, *15*, 3320–3329.
- (31) Uzun, S.; Seyedin, S.; Stoltzfus, A. L.; Levitt, A. S.; Alhabeb, M.; Anayee, M.; Strobel, C. J.; Razal, J. M.; Dion, G.; Gogotsi, Y. Knittable

- and Washable Multifunctional MXene-Coated Cellulose Yarns. Adv. Funct. Mater. 2019, 29, 1905015.
- (32) Yun, T.; Kim, H.; Iqbal, A.; Cho, Y. S.; Lee, G. S.; Kim, M. K.; Kim, S. J.; Kim, D.; Gogotsi, Y.; Kim, S. O.; Koo, C. M. Electromagnetic Shielding of Monolayer MXene Assemblies. *Adv. Mater.* **2020**, 32, No. e1906769.
- (33) Han, M.; Shuck, C. E.; Rakhmanov, R.; Parchment, D.; Anasori, B.; Koo, C. M.; Friedman, G.; Gogotsi, Y. Beyond Ti3C2Tx: MXenes for Electromagnetic Interference Shielding. *ACS Nano* **2020**, *14*, 5008–5016.
- (34) Hantanasirisakul, K.; Gogotsi, Y. Electronic and Optical Properties of 2D Transition Metal Carbides and Nitrides (MXenes). *Adv. Mater.* **2018**, *30*, No. e1804779.
- (35) Lin, H.; Gao, S.; Dai, C.; Chen, Y.; Shi, J. A Two-Dimensional Biodegradable Niobium Carbide (MXene) for Photothermal Tumor Eradication in NIR-I and NIR-II Biowindows. *J. Am. Chem. Soc.* **2017**, 139, 16235–16247.
- (36) Ding, L.; Wei, Y.; Wang, Y.; Chen, H.; Caro, J.; Wang, H. A Two-Dimensional Lamellar Membrane: MXene Nanosheet Stacks. *Angew. Chem., Int. Ed. Engl.* **2017**, *56*, 1825–1829.
- (37) Karlsson, L. H.; Birch, J.; Halim, J.; Barsoum, M. W.; Persson, P. O. Atomically Resolved Structural and Chemical Investigation of Single MXene Sheets. *Nano Lett.* **2015**, *15*, 4955–4960.
- (38) Srivastava, P.; Mishra, A.; Mizuseki, H.; Lee, K. R.; Singh, A. K. Mechanistic Insight into the Chemical Exfoliation and Functionalization of Ti3C2 MXene. ACS Appl. Mater. Interfaces 2016, 8, 24256—24264.
- (39) Osti, N. C.; Naguib, M.; Ostadhossein, A.; Xie, Y.; Kent, P. R.; Dyatkin, B.; Rother, G.; Heller, W. T.; van Duin, A. C.; Gogotsi, Y.; Mamontov, E. Effect of Metal Ion Intercalation on the Structure of MXene and Water Dynamics on its Internal Surfaces. ACS Appl. Mater. Interfaces 2016, 8, 8859–8863.
- (40) Zhang, J.; Kong, N.; Uzun, S.; Levitt, A.; Seyedin, S.; Lynch, P. A.; Qin, S.; Han, M.; Yang, W.; Liu, J.; Wang, X.; Gogotsi, Y.; Razal, J. M. Scalable Manufacturing of Free-Standing, Strong Ti3 C2 Tx MXene Films with Outstanding Conductivity. *Adv. Mater.* **2020**, *32*, 2001093.
- (41) Wang, X.; Wang, Z.; Qiu, J. Stabilizing MXene by Hydration Chemistry in Aqueous Solution. *Angew. Chem., Int. Ed.* **2021**, *60*, 26587–26591.
- (42) Wu, T.; Kent, P. R. C.; Gogotsi, Y.; Jiang, D.-e. How Water Attacks MXene. *Chem. Mater.* **2022**, *34*, 4975–4982.
- (43) Chen, L.; Dai, X.; Feng, W.; Chen, Y. Biomedical Applications of MXenes: From Nanomedicine to Biomaterials. *Acc. Mater. Res.* **2022**, *3*, 785–798.
- (44) Huang, K.; Li, Z.; Lin, J.; Han, G.; Huang, P. Two-dimensional transition metal carbides and nitrides (MXenes) for biomedical applications. *Chem. Soc. Rev.* **2018**, *47*, 5109–5124.
- (45) Lin, H.; Chen, Y.; Shi, J. Insights into 2D MXenes for Versatile Biomedical Applications: Current Advances and Challenges Ahead. *Adv. Sci.* **2018**, *5*, 1800518.
- (46) Amara, U.; Hussain, I.; Ahmad, M.; Mahmood, K.; Zhang, K. 2D MXene-Based Biosensing: A Review. Small 2023, 19, 2205249.
- (47) Iravani, S.; Varma, R. S. MXenes in photomedicine: advances and prospects. *Chem. Commun.* **2022**, *58*, 7336–7350.
- (48) Wu, L.; You, Q.; Shan, Y.; Gan, S.; Zhao, Y.; Dai, X.; Xiang, Y. Few-layer Ti3C2Tx MXene: A promising surface plasmon resonance biosensing material to enhance the sensitivity. *Sens. Actuators, B* **2018**, 277, 210–215.
- (49) Wang, Y.; Garg, R.; Cohen-Karni, D.; Cohen-Karni, T. Neural modulation with photothermally active nanomaterials. *Nat. Rev. Bioeng.* **2023**, 1–15.
- (50) Siwal, S. S.; Kaur, H.; Chauhan, G.; Thakur, V. K. MXene-Based Nanomaterials for Biomedical Applications: Healthier Substitute Materials for the Future. *Adv. NanoBiomed Res.* **2023**, *3*, 2200123.
- (51) Mathis, T. S.; Maleski, K.; Goad, A.; Sarycheva, A.; Anayee, M.; Foucher, A. C.; Hantanasirisakul, K.; Shuck, C. E.; Stach, E. A.; Gogotsi, Y. Modified MAX Phase Synthesis for Environmentally

- Stable and Highly Conductive Ti3C2 MXene. ACS Nano 2021, 15, 6420-6429.
- (52) Naguib, M.; Barsoum, M. W.; Gogotsi, Y. Ten Years of Progress in the Synthesis and Development of MXenes. *Adv. Mater.* **2021**, 33, No. e2103393.
- (53) Wei, Y.; Zhang, P.; Soomro, R. A.; Zhu, Q.; Xu, B. Advances in the Synthesis of 2D MXenes. *Adv. Mater.* **2021**, 33, No. e2103148.
- (54) Kamysbayev, V.; Filatov, A. S.; Hu, H.; Rui, X.; Lagunas, F.; Wang, D.; Klie, R. F.; Talapin, D. V. Covalent surface modifications and superconductivity of two-dimensional metal carbide MXenes. *Science* **2020**, *369*, 979–983.
- (55) Chae, Y.; Kim, S. J.; Cho, S. Y.; Choi, J.; Maleski, K.; Lee, B. J.; Jung, H. T.; Gogotsi, Y.; Lee, Y.; Ahn, C. W. An investigation into the factors governing the oxidation of two-dimensional Ti3C2 MXene. *Nanoscale* **2019**, *11*, 8387–8393.
- (56) Li, G.; Tan, L.; zhang, Y.; Wu, B.; Li, L. Highly Efficiently Delaminated Single-Layered MXene Nanosheets with Large Lateral Size. *Langmuir* **2017**, *33*, 9000–9006.
- (57) Sarycheva, A.; Gogotsi, Y. Raman Spectroscopy Analysis of the Structure and Surface Chemistry of Ti3C2Tx MXene. *Chem. Mater.* **2020**, *32*, 3480–3488.
- (58) Weber, R. E. Use of ionic and zwitterionic (Tris/BisTris and HEPES) buffers in studies on hemoglobin function. *J. Appl. Physiol.* **1992**, 72, 1611–1615.
- (59) Cook, S. R.; Badell-Grau, R. A.; Kirkham, E. D.; Jones, K. M.; Kelly, B. P.; Winston, J.; Waller-Evans, H.; Allen, N. D.; Lloyd-Evans, E. Detrimental effect of zwitterionic buffers on lysosomal homeostasis in cell lines and iPSC-derived neurons. *AMRC Open Res.* **2020**, *2*, 21.
- (60) Yu, Q.; Kandegedara, A.; Xu, Y.; Rorabacher, D. B. Avoiding interferences from Good's buffers: A contiguous series of noncomplexing tertiary amine buffers covering the entire range of pH 3-11. *Anal. Biochem.* **1997**, 253, 50–56.
- (61) Shuck, C. E.; Sarycheva, A.; Anayee, M.; Levitt, A.; Zhu, Y.; Uzun, S.; Balitskiy, V.; Zahorodna, V.; Gogotsi, O.; Gogotsi, Y. Scalable Synthesis of Ti3C2Tx MXene. *Adv. Eng. Mater.* **2020**, 22, 1901241.
- (62) Maleski, K.; Shuck, C. E.; Fafarman, A. T.; Gogotsi, Y. The Broad Chromatic Range of Two-Dimensional Transition Metal Carbides. *Adv. Opt. Mater.* **2021**, *9*, 2001563.
- (63) Valurouthu, G.; Maleski, K.; Kurra, N.; Han, M.; Hantanasirisakul, K.; Sarycheva, A.; Gogotsi, Y. Tunable electro-chromic behavior of titanium-based MXenes. *Nanoscale* **2020**, *12*, 14204–14212.
- (64) Lukatskaya, M. R.; Mashtalir, O.; Ren, C. E.; Dall'Agnese, Y.; Rozier, P.; Taberna, P. L.; Naguib, M.; Simon, P.; Barsoum, M. W.; Gogotsi, Y. Cation intercalation and high volumetric capacitance of two-dimensional titanium carbide. *Science* **2013**, *341*, 1502–1505.
- (65) Shekhirev, M.; Shuck, C. E.; Sarycheva, A.; Gogotsi, Y. Characterization of MXenes at every step, from their precursors to single flakes and assembled films. *Prog. Mater. Sci.* **2021**, *120*, 100757.
- (66) Cockreham, C. B.; Zhang, X.; Eakin, J. A.; Dewa, M.; Li, H.; Li, N.; Sun, J.; Ha, S.; Ivory, C. F.; Wang, Y.; Xu, H.; Wu, D. Unveiling the Interfacial and Structural Heterogeneity of Ti3C2Tx MXene Etched with CoF2/HCl by Integrated in Situ Thermal Analysis. ACS Appl. Mater. Interfaces 2021, 13, 52125–52133.